Journal of Solid State Chemistry 184 (2011) 2559–2565

Contents lists available at ScienceDirect

Journal of Solid State Chemistry

journal homepage: www.elsevier.com/locate/jssc

Thermal expansion behaviour in the oxygen deficient perovskites $Sr_2BSbO_{5.5}$ (B=Ca, Sr, Ba). Competing effects of water and oxygen ordering

Qingdi Zhou [a], Brendan J. Kennedy [a,*], Maxim Avdeev [b]

[a] School of Chemistry, The University of Sydney, Sydney, NSW 2006, Australia
[b] Bragg Institute, Australian Nuclear Science and Technology Organisation, Private Mail Bag 1, Menai, NSW 2234, Australia

ARTICLE INFO

Article history:
Received 11 April 2011
Received in revised form
28 June 2011
Accepted 6 July 2011
Available online 27 July 2011

Keywords:
Oxygen vacancies
Disorder
Thermal expansion
Perovskite

ABSTRACT

Neutron diffractions studies reveal the presence of oxygen disorder in the oxygen deficient perovskites $Sr_2BSbO_{5.5}$ (B=Ca, Sr, Ba). Synchrotron X-ray studies demonstrate that these oxides have a double perovskite-type structure with the cell size increasing as the size of the B cation increases from 8.2114(2) Å for B=Ca to 8.4408(1) Å for B=Ba. It is postulated that a combination of local clustering of the anions and vacancies together with water–water and water–host hydrogen bonds plays a role in defining the volume of the encapsulated water clusters and that changes in the local structure upon heating result in anomalous thermal expansion observed in variable temperature diffraction measurements.

1. Introduction

A major barrier to the wide-scale utilisation of solid oxide fuel cells (SOFCs) is the development of an anode material that has low electrode overpotentials and ohmic losses at relatively low temperatures and that will operate with a range of fuels, in particular natural gas. Anion deficient perovskite-type oxides of the type ABO_{3-x} are currently amongst the most promising materials for such applications, and considerable effort is being directed to their study [1,2]. A key feature of the perovskite structure is its ability to incorporate a large range of metals on either the A- or B-type sites, allowing for optimisation of the targeted physical properties. Recent work in this area has included studies of a number of oxygen deficient double perovskites of the type $A_2BB'O_{6-x}$ where two different cations exhibit a rock-salt like ordering in the octahedral lattice [2,3]. In addition to oxide ion conductivity the same anion deficient perovskites can exhibit proton conductivity under wet atmospheres as a consequence of their ability to incorporate water [1,4,5]. Indeed $Sr_3NbO_{5.5}$ is reported to become a proton conductor after absorbing water at moderate temperatures [6]. Anion deficient double perovskites also show promise as photocatalysts for water splitting [7].

Niobium and tantalum both form a series of double perovskites that can be described by the general formula $Sr^{II}_{6-2x}B^{V}_{2+2x}O_{11+3x}$ (B=Nb, Ta) that simplifies to $Sr_3BO_{5.5}$ when x=0. These oxides are structurally related to the rare mineral cryolite Na_3AlF_6 in which the Na^+ cation occupies both the A and half the B-sites of the perovskite [8]. Stoichiometric analogues such as Sr_3WO_6 are also known [9,10]. Levin and co-workers [11] have demonstrated that $Sr_4Nb_2O_9$, the x=1/3 member of the series $Sr^{II}_{6-2x}Nb^{V}_{2+2x}O_{11+3x}$, exhibits a cryolite-like structure with Sr and Nb ordering on the perovskite B sites. These workers concluded that the material exhibits a complicated local structure with disorder of both the anion and perovskite A-type Sr cations. They also noted that the precise composition of $Sr_4Nb_2O_9$ was sensitive to annealing conditions suggesting that there may be anion and/or A-site vacancies. Li and Hong [12] explored this suggestion and these authors established both that the oxygen anions partially occupy interstitial sites in the perovskite and that the distribution of the anions was dependent on the precise stoichiometry. A number of other cryolite-like oxides including $Ba_4Ca_2Nb_2O_{11}$ ($Ba_2CaNbO_{5.5}$) and $Ba_4Ca_2Ta_2O_{11}$ ($Ba_2CaTaO_{5.5}$) have recently been shown to exhibit high proton conductivity [13–16].

Following the early report of the preparation of $Sr_{(1.45-x)}Ca_xSb_{0.55}O_{3-y}$ [17] Chinarro and co-workers [18] recently reported the synthesis and characterisation of $Sr_3SbO_{5.5}$, the x=0 member of the series $Sr^{II}_{6-2x}Sb^{V}_{2+2x}O_{11+3x}$. Although X-ray diffraction measurements suggested a random distribution of the oxygen vacancies, their electron microscopy studies suggested the presence of short-range ordering of the oxygen vacancies. Finally they concluded that, at moderate oxygen partial pressures $pO_2 < 10^{-1.25}$ atm, the presence of oxygen vacancies gave rise to oxide ion conductivity.

* Corresponding author. Fax: +61 2 9351 3329.
E-mail address: b.kennedy@chem.usyd.edu.au (B.J. Kennedy).

0022-4596/$ - see front matter © 2011 Elsevier Inc. All rights reserved.
doi:10.1016/j.jssc.2011.07.019

In the present work we have used a variety of diffraction experiments to study the temperature dependence of the structures of the three oxides $Sr_2BSbO_{5.5}$ (B=Ca, Sr or Ba). The aim of this work is to establish if anion disorder is present in these oxides, and if so, how this is affected by the choice of A-site cation.

2. Experimental

Samples of $Sr_2BSbO_{5.5}$ (B=Ca, Sr or Ba) were prepared using a method similar to that described by Chinarro and co-workers [18]. Appropriate stoichiometric amounts of Sb_2O_3 (Aldrich 99.99%), $SrCO_3$ (Aldrich 99.9+%), $BaCO_3$ (Aldrich 99.98%) and $CaCO_3$ (Aldrich 99.95%) were intimately mixed and fired at 850 °C for 16 h. The samples were then reground and heated at 1100 °C for 48 h.

Thermal gravimetric analyses were performed using a Hi-Res TGA 2950 Thermogravimetric Analyzer with a 1.5 g capacity and high balance sensitivity (0.1 μg). All samples were measured in the temperature range 30–700 °C under oxygen of purge rate 40 and 60 mL/min, at a heating rate of 10 °C/min. The calculations of weight lost were performed using the Universal Analysis 2000 (Version 4.2E) programme.

Variable temperature powder X-ray diffraction data were collected on a PANalytical X'Pert PRO X-ray diffractometer using Cu $K\alpha$ radiation and a PIXcel solid-state detector. Temperature control was achieved using an XRK 900 Reactor Chamber, operating under a vacuum of 10^{-3} Torr . The sample was allowed to equilibrate for 5 min after reaching each measurement temperature. Each pattern took around 8 min to collect. The structure was refined by the Rietveld method implemented in the programme Rietica [19] using data in the range $15^\circ \le 2\theta \le 90^\circ$. The peak profiles were fitted using a pseudo-Voigt function coupled with an asymmetry function.

Room-temperature synchrotron X-ray powder diffraction patterns were collected on the high-resolution Debye–Scherrer diffractometer at beamline 20B, the Australian National Beamline Facility, Photon Factory, Japan [20]. The wavelength was set at λ=0.82606 Å (determined using NIST silicon Standard Reference Material 640c). The samples were finely ground and loaded into 0.3 mm glass capillaries that were continuously rotated during the measurements. Data were recorded using three BAS2000 Fuji image plates as detectors. Each image plate is 20×40 cm and each covers 40° in 2θ, allowing data to be collected over the range 2θ=5–125° with a step size of 0.01005°. A thin strip ca. 0.5-cm wide is used to record each diffraction pattern. All measurements were performed under vacuum to minimise air scatter. A pseudo-Voigt function was used to model the peaks. The background was estimated by linear interpolation between regions where there were no Bragg peaks.

Neutron powder diffraction data of the samples were measured at room temperature using the high-resolution powder diffractometer Echidna at ANSTO's OPAL facility at Lucas Heights [21]. The data were collected using a wavelength of 1.538 Å over the range 2θ=10–160° with a step size of 0.05°. For these measurements the sample was contained in a cylindrical vanadium can. A pseudo-Voigt function with asymmetry correction was used to model the peaks.

3. Results and discussion

3.1. Thermogravimetric analysis

The TGA measurements show the presence of at least three events for each of the samples (Fig. 1). The initial weight loss at temperatures of ≤100 °C is thought to be due to the loss of chemisorbed water, whilst the weight loss near 300 °C is due to the removal of the water molecules that occupied the anion vacancies. Attempts to quantify the water loss using infra-red measurements were unsuccessful. At still higher temperatures all the samples displayed significant weight loss [13]. Diffraction measurements indicated that, when heated under vacuum, the samples decomposed above 700 °C.

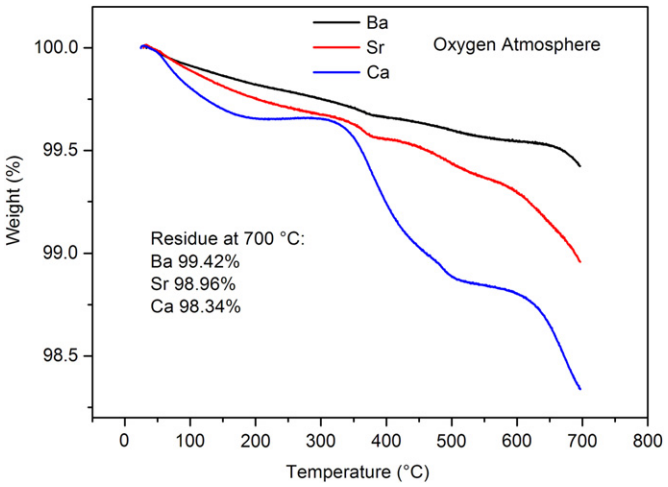

Fig. 1. Thermogravimetric curves for the three oxides $Sr_2BSbO_{5.5}nH_2O$ measured under a dry oxygen atmosphere.

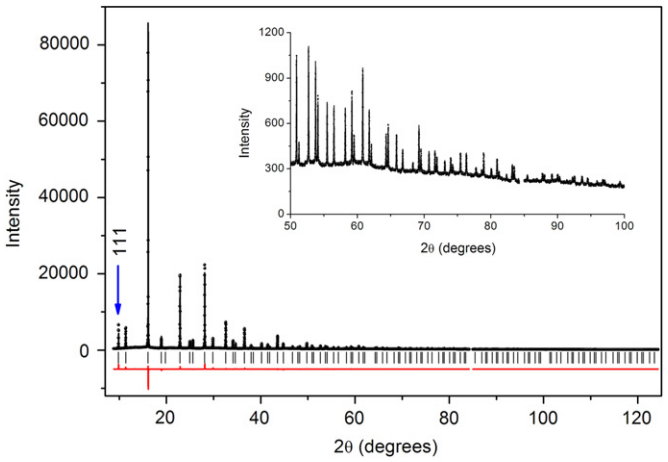

Fig. 2. Observed, calculated and difference synchrotron X-ray diffraction profiles for $Sr_3SbO_{5.5}$ at room temperature. The inset highlights the quality of the fit to higher angle. The data were collected with λ=0.82606 Å.

3.2. Room temperature structures

The synchrotron X-ray powder diffraction patterns of the three $Sr_2BSbO_{5.5}nH_2O$ (B=Ca, Sr or Ba) samples exhibited strong (1 1 1) reflections indicative of 1:1 ordering of the two B-site cations (Fig. 2). No splitting or asymmetry of the cubic reflections was detected in the diffraction patterns up to 2θ=125° demonstrating that the structures were all cubic, and the appropriate space group was $Fm\bar{3}m$ with $a \sim 8.3$ Å. As expected the cell size increases as the size of the B cation increases from 8.2114(2) Å for B=Ca to 8.4408(1) Å for B=Ba. The lattice parameter for $Sr_3SbO_{5.5}$ is essentially the same as that reported by Chinarro and co-workers [18] who demonstrated the Sb to be pentavalent.

In the double perovskite structure it is anticipated that the two smallest cations will order in the octahedral sites, this ordering

being a consequence of the differences in the size and/or charge between the two cations. The largest cation will then occupy the 12-coordinated (cuboctahedral) site. For $Sr_2CaSbO_{5.5}$ the appropriate ionic radii are Sr^{2+} (12-coord. 1.44; 6-coord. 1.18 Å); Ca^{2+} (1.34 and 1.00 Å) and Sb^{5+} (6-coord. 0.60 Å [22]) suggesting the Ca^{2+} and Sb^{5+} cations will occupy the 6-coordinate sites and the Sr^{2+} the 12 coordinate sites [22]. The corresponding sizes of Ba^{2+} (12-coord.1.61 Å and 6-coord. 1.35 Å), suggest that in $Sr_2BaSbO_{5.5}$ the Sb^{5+} and one Sr^{2+} will occupy the 6-coordinate sites and the cuboctahedral sites will be occupied by a mixture of Sr^{2+} and Ba^{2+}.

The Rietveld refinements using the synchrotron X-ray powder diffraction data confirmed the ordering of the two *B*-site cations and established the distribution of these. Refinement of the structure of $Sr_2CaSbO_{5.5}$, assuming the Ca only occupies the octahedral sites gave R_p=6.05% and R_{wp}=5.52%. Refinements where the Ca and Sr were allowed to disorder over the two appropriate sites (anti-site disorder) did not significantly alter the quality of the fits R_p=6.10% and R_{wp}=5.46% and indicated that less than 5% of the Ca was in the cuboctahedral sites. Likewise the refinements of the structure of $Sr_2BaSbO_{5.5}$ provide no evidence for mixing of the Sr and Ba cations over the 6- and 12-coordinate sites, with the ideal model (all Ba^{2+} in the cuboctahedral sites) having R_p=4.38 and R_{wp}=4.77% and the anti-site disordered model gives identical *R*-values and has Ba occupancy of the octahedral site within 1 esd of zero. In these refinements it was assumed that all the Sb^{5+} remains in the octahedral sites and that there is no anti-site disorder across the crystallographically distinct octahedral sites. Anomalous dispersion measurements would be needed to test this assumption. In the final refinement cycles and in refinements using the powder neutron diffraction data (see below) we assumed an ideal cation distribution.

While the synchrotron X-ray diffraction data provides a good description of the bulk structure, the refinements were relatively insensitive to the precise anion positions and in particular to the nature of the non-stoichiometry. Accordingly high-resolution neutron diffraction patterns for the three samples were obtained to better understand this. A striking feature of the neutron diffraction profiles for $Sr_3SbO_{5.5}$ and $Sr_2CaSbO_{5.5}$ is the presence of diffuse intensity in the form of a modulated background (Fig. 3). Since there is only one anion site in the ideal cryolite structure it is not possible to have an ordered arrangement of the

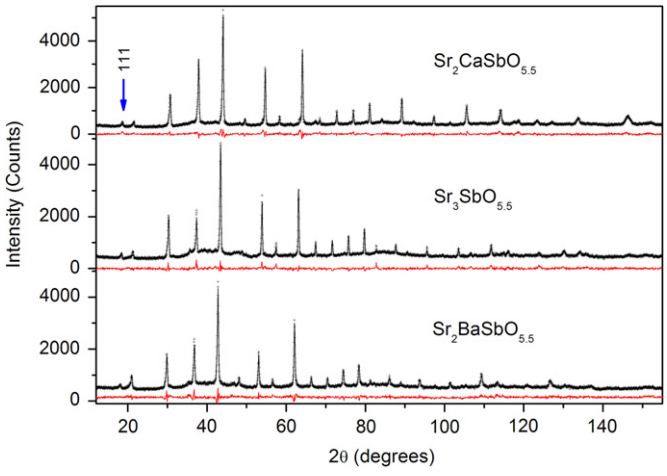

Fig. 3. Rietveld plots for neutron diffraction patterns recorded at room temperature for the three $Sr_2ASbO_{5.5}$ samples fitted in $Fm\bar{3}m$. The crosses represent the observed diffraction data, and the solid line joining them the calculated profile. The lower traces are the difference plots. The data were collected with λ=1.538 Å.

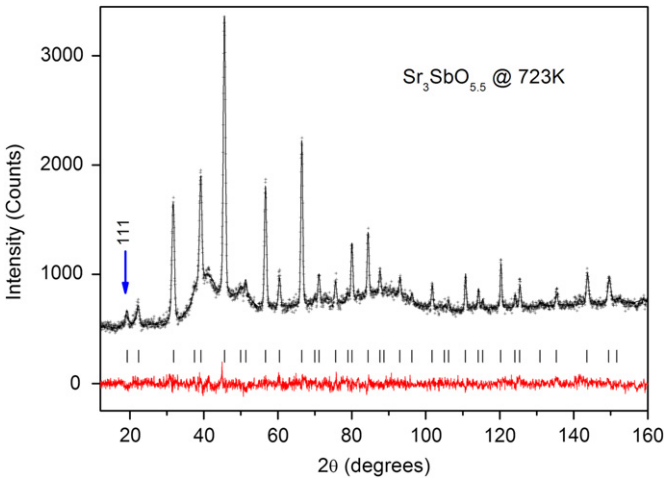

Fig. 4. Observed, calculated and difference neutron diffraction profiles for $Sr_3SbO_{5.5}$ at 723 K. At this temperature the sample is fully dehydrated and the diffuse background is a result of oxygen disorder.

vacancies. The observed backgrounds are similar to that reported by Levin and co-workers for $Sr_4Nb_2O_9$ [11]. This diffuse structure was not immediately apparent in the synchrotron X-ray profiles where the samples were contained in glass capillaries that themselves contribute a modulated background to the patterns, but very weak features could be identified in the X-ray diffraction patterns collected using a Bragg–Brentano X-ray diffractometer. That the modulated background is much stronger in the neutron profile compared to the X-ray patterns suggests it is associated with disorder of the lighter atoms. *Ex-situ* dehydration of $Sr_2CaSbO_{5.5}$ did not significantly alter the appearance or relative intensity of the background in the neutron diffraction patterns demonstrating that this is not due to the presence of absorbed water in the samples. Neutron diffraction data were collected for $Sr_3SbO_{5.5}$ at 373, 473, 573, 673 and 723 K, and as is evident from Fig. 4 the strong diffuse background remains present even at the highest of these temperatures. Neutron diffraction studies of other defect perovskites of the type $Ba_2LnSn_{1-x}Sb_xO_{6-d}$ did not reveal similar diffuse backgrounds [23] demonstrating non-stoichiometry alone is not a sufficient condition for this.

Initial refinements of the structure of $Sr_3SbO_{5.5}$ against the neutron diffraction data using the model developed in the analysis of the synchrotron data yielded very poor fits, R_p=6.42 and R_{wp}=9.92%, and abnormally large values of the atomic displacement parameters (ADP). The large ADP suggest displacements of some ions from their special positions, and as noted by Levin [11] short-range correlations between such displacements could give rise to the modulated diffuse background. The fits to the neutron diffraction profile was improved by introducing positional disorder (displacive disorder) of both the cuboctahedral, Sr, cations and the oxygen anions but the resulting fits remained unsatisfactory. Displacive disorder of the *A*-type cation has been observed in a number of perovskites, especially those containing Pb [24]. The *A*-type cations were located on the 32*f* sites at (*x x x*) *x*∼¼, and the occupancy of this site set to ¼ to maintain the stoichiometry of the sample. Examination of the Fourier maps generated by Rietica revealed the presence of nuclear density near 0 1/6 1/6, corresponding to a 48*h* site in $Fm\bar{3}m$. Allowing oxygen to partially occupy these sites resulted in a dramatic improvement in the quality of the fit in the various measures of fit R_p=4.55% and R_{wp}=6.00%, although a number of weak reflections remained poorly fitted and the ADP remained unusually large. The use of anisotropic displacement parameters for the O(1) anion at (*x* 0 0) further improved the quality of the fit.

The anisotropy corresponds to the libration of the BO_6 octahedra. The large displacement parameters suggest the local distortions are similar to those associated with tilting of the octahedra that lowers the symmetry. In general terms, tensile stress of the *A*–O bonds in ABO_3 perovskites that arises due to a mismatch in size of the *A*- and *B*-type cations is relieved by tilting of the octahedra. The rotation of the BO_6 octahedra is accompanied by distortion of the oxygen coordination sphere around the *A*-cation and, in certain symmetries, displacements of the *A*-cations from their ideal positions. In the present case the displacement of the *A*-cations occurs in the absence of long-range tilting of the BO_6 octahedra, although the large anisotropic displacement parameters of the oxygen anions hint that such tilting may occur over a short range.

Finally the possibility of displacive disorder of the octahedrally coordinated Sr and Sb cations was considered. No evidence was found for displacive disorder of the cation on the 4*a* site (0, 0, 0), but a ⟨0 1 1⟩ displacement of the 4*b* cation at ½ ½ ½ onto a 48*i* site at ½ *y y* with $y \sim 0.5$ gave an optimal fit to the neutron data. The occupancy of the 48*i* site was fixed in the refinements to give the required stoichiometry. The same model provided a good fit to the synchrotron X-ray diffraction data. We are unaware of many examples of displacive disorder of *B*-type cations in ABO_3 perovskites although similar disorder has been observed in the defect perovskite $Ba_{11}W_4O_{23}$ by Hong [25]. Although not explicitly discussed by Hong the neutron diffraction profile of $Ba_{11}W_4O_{23}$ also exhibits a structured background. Attempts to locate the hydrogen atoms from the water molecules were unsuccessful. Presumably this is a consequence of both the small amount of water present in the sample and the disorder evident in the structure. No constraints were placed on the oxygen stoichiometry in the final refinement cycles. The total refined oxygen contents were 5.83(12), 5.48(14) and 5.40(12) for *B*=Ca, Sr and Ba, respectively. These values are reasonably consistent with the corresponding water occupancies estimated from the TGA measurements $n=0.245$, 0.174 and 0.112. The increased amount of water incorporated into the $Sr_2CaO_{5.5}$ lattice, relative to the other two oxides may account for the differences in the thermal expansion described below. The final refined parameters are tabulated in Table 1, and the structure is illustrated in Fig. 5.

The same model was used to refine a structure for $Sr_2BaSbO_{5.5}$. The diffuse structure in the neutron diffraction pattern for $Sr_2CaSbO_{5.5}$ was noticeably less obvious than for the other two compounds (see Fig. 3) and in this case it was possible to obtain a satisfactory fit to both the neutron and synchrotron X-ray diffraction data to a model where all the oxygen was located on the 24*e* (*x* 0 0) site and there was no displacive disorder of the Sb from the 4*b* site to the nearby 48*i* site. The refinements still suggest the presence of displacive disorder of the Sr on the perovskites *A*-type sites onto the 32*f* site.

The anion disorder observed in $Sr_2BaSbO_{5.5}$ and $Sr_3SbO_{5.5}$ is similar to that found by Li and Hong [12] in $Sr_{6-2x}Nb_{2+2x}O_{11+3x}$ ($x=0.103$) and in $Sr_4Nb_2O_9$ by Levin and co-workers [11], who also concluded that displacive disorder of the Sr on the perovskite *A*-site was also present. It appears likely that this is a characteristic feature of such oxides, and the only reason it is not generally recognised is the reliance of most researchers on X-ray, rather than neutron, diffraction methods to structurally characterise their samples.

Table 2 lists selected bond distances obtained from the structural refinements. Whilst the refinements provide an adequate description of the average structure, perusal of this table shows some physically unrealistic bond distances, for example the average Ca–O2 distance of 2.05 Å. The need to for shorter than typical Ca–O bonds is evident from Bond Valence Sum calculations. The displacements of the various ions from their ideal positions will undoubtedly be coupled and the use of methods more sensitive to local structural distortions such as EXAFS or PDF analysis is likely to be informative [26].

Table 1
Unit cell and structural and isotropic atomic displacement (*B*) parameters, for $Sr_2BO_{5.5}nH_2O$ from Rietveld refinements using powder neutron diffraction data recorded at room temperature. The refined occupancy factors (*n*) for each site are also listed; where these are not given the site is fully occupied by the listed ion. The structures were refined in space group $Fm\bar{3}m$. Anisotropic ADP were only refined for *O*(1), and these values together with the values obtained assuming isotropic displacements for this anion are tabulated.

	Wyckoff site	Parameter	$Sr_2CaSbO_{5.5}$	$Sr_3SbO_{5.5}$	$Sr_2BaSbO_{5.5}$
nH_2O[a]			0.245	0.174	0.112
a (Å)			8.1962(2)	8.3104(3)	8.4354(4)
A	32*f* (*x x x*)	*x*	0.238(4)	0.232(2)	0.236(4)
		B_{iso} (Å^2)	2.5(5)	4.1(4)	3.6(6)
		*n*Sr	2.00	2.00	1.00
B	4*a* (0 0 0)	B_{iso} (Å^2)	0.64(7)	1.99(8)	1.72(6)
		*n*Sr	0.00	1.00	1.00
B′(Sb)[b]	48*i* (½ *y y*)	*y*	½	0.5380(9)	0.5352(6)
		B_{iso} (Å^2)	2.75(12)	2.1(4)	1.72(6)
O(1)	24*e* (*x* 0 0)	*x*	0.2338(3)	0.2484(7)	0.2510(8)
		B_{11} (Å^2)	3.7(4)	10.5(6)	10.1(6)
		$B_{22}=B_{33}$ (Å^2)	42.2(6)	25.3(5)	19.4(4)
		B_{iso} (Å^2)	5.92(10)	4.22(7)	3.48(7)
		n	5.12(6)	4.18(7)	4.61(6)
O(2)	48*h* (0 *y y*)	*y*	0.1672(10)	0.1606(9)	0.1613(13)
		B_{iso} (Å^2)	3.1(3)	2.5(2)	6.1(6)
		n	0.71(6)	1.30(7)	0.79(7)
R_p			4.95	4.66	4.28
R_{wp}			6.51	5.92	5.45
χ^2			2.09	1.94	1.78

[a] Water content from DTA.
[b] In $Sr_2CaSbO_{5.5}$ the Sb is on the 4*b* site at (½ ½ ½).

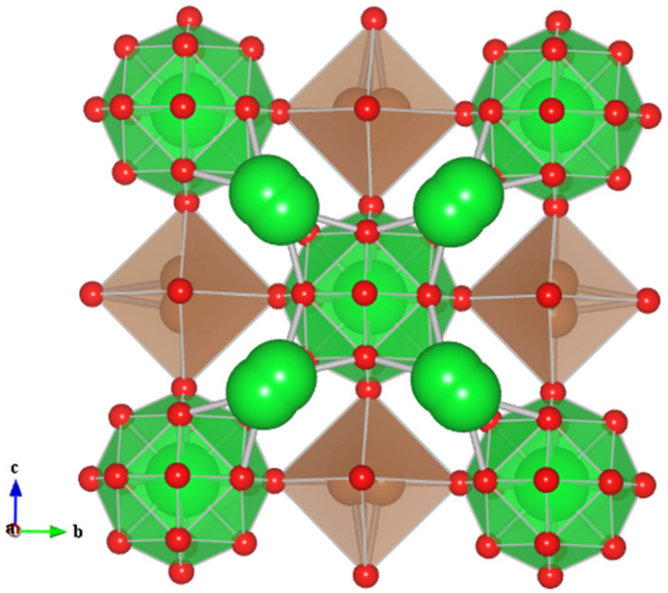

Fig. 5. Representation of the structure of $Sr_3SbO_{5.5}$ obtained from the refinements against neutron diffraction data. The small red spheres are the oxygen anions, and the tan octahedra are the SbO_6 groups. The large green spheres represent the Sr cations, and the associated disordered SrO_6 groups. The unusual shape of the overlapping spheres is a consequence of the displacive disorder. (For interpretation of the references to colour in this figure legend, the reader is referred to the web version of this article.)

Table 2
Selected bond distances for $Sr_2BO_{5.5}nH_2O$ from Rietveld refinements using powder neutron diffraction data recorded at room temperature. The average A–O_{av} and Sb–O_{av} distances were estimated for a single disordered cation.

	$Sr_2CaSbO_{5.5}$	$Sr_3SbO_{5.5}$	$Sr_2BaSbO_{5.5}$
A–O1$_{av}$ (Å)	2.908(3)	2.9627(6)	2.986
A–O2$_{av}$ (Å)	2.05(3)	1.959(3)	2.311
B–O1 (Å)	2.056(9)	2.117(7)	2.115(8)
B–O2 (Å)	1.94(1)	1.952(7)	1.964(13)
Sb–O1$_{av}$ (Å)	2.042(9)	2.038(7)	2.021(6)
Sb–O2$_{av}$ (Å)	3.052(3)	3.099(2)	3.156(4)
O1–O2 (Å)	1.533(6)	1.565(4)	1.603(4)
O2–O2 (Å)	1.939(11)	1.952(7)	1.949(11)

The absence of tilting in the present oxides is surprising given the estimated tolerance factors defined as $t=(R_A+R_O)/\sqrt{2}(R_B+R_O)$ where R_A, R_B, and R_O are the ionic radii of the 12-coordinate A site and 6-coordinate B site cations (appropriately weighted for the observed cation distribution) and the oxygen ion, respectively, are all well less than unity. The measured neutron (and synchrotron X-ray) diffraction profiles show no evidence for superlattice reflections associated with such tilts. In general terms tolerance factors of less than one result in significant underbonding of the A-site cation. Bond valence sum calculations of the ideal model – that is where there is no displacive disorder of the A-type cations and the only the 24e anion site is occupied – confirmed this. The combination of displacive disorder and anion vacancies precludes meaningful bond valence analysis of the structures, however these establish that occupancy of the 48h site, that results in shorter A–O distances, can alleviate this underbonding. It appears that the displacive disorder of the cations, together with the anion vacancies is sufficient to relieve the apparent bonding instabilities estimated from the average structure. Levin and co-workers noted tilting was also absent in $Sr_3NbO_{5.5}$, which also exhibits displacive disorder of the cations and a random distribution of anion vacancies [11].

3.3. Variable temperature XRD

Powder X-ray diffraction patterns were recorded for the three $Sr_2BSbO_{5.5}nH_2O$ samples between room temperature and 500 °C using a conventional Cu X-ray source. The structures of the three samples remained cubic over this temperature range. Heating to higher temperatures resulted in some decomposition in the samples with B=Ba or Sr as has also been observed in the related Nb and Ta oxides $Sr_3BO_{5.5}$ (B=Nb, Ta) [14].

As is evident from Fig. 6 the behaviour of the Sr and Ba oxides are essentially that same but these are somewhat different to that exhibited by the Ca sample. In all cases the cell parameter shows an initial almost linear increase as the temperature is increased, followed by a noticeable increase in the rate of thermal expansion, before the lattice parameter plateaus, or in the case of $Sr_2CaSbO_{5.5}$, shows an obvious decrease. Heating the sample to still higher temperatures results in a return to almost linear thermal expansion behaviour. The temperature at which the cell size begins to decrease depends on the size of the B-type cation, increasing in the order Ca < Sr < Ba. The TGA results, described above, demonstrated that the samples exhibit a small weight loss near 250–300 °C and the temperature at which this occurred increased in the same order, suggesting the two events are related. It is expected that the loss of water from the structure would lead to a contraction of the cell size, and recent diffraction studies of hydrated pyrochlores have

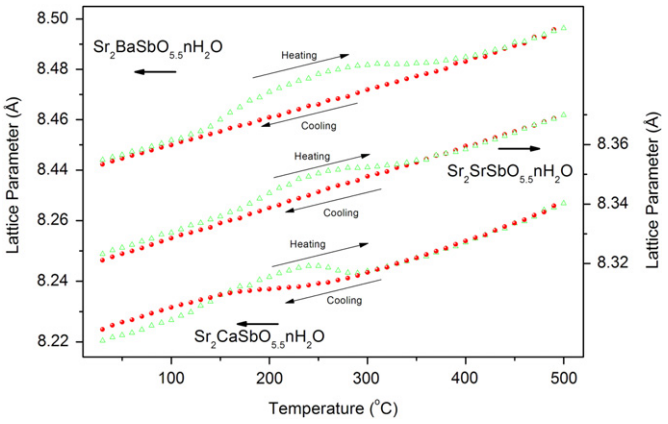

Fig. 6. Temperature dependent lattice parameters for the three oxides $Sr_2BSbO_{5.5}nH_2O$ (B=Ca, Sr and Ba). The green triangles are the results obtained during the heating cycle and the red circles those during cooling. The sample vacuum was $\sim 1\times10^{-3}$ Torr during the measurements. Note the offset in y-axis between the three samples used to highlight the variations. (For interpretation of the references to colour in this figure legend, the reader is referred to the web version of this article.)

demonstrated this [27]. The observation that loss of water coincides with the increased rate of thermal expansion of the lattice parameters is unexpected and points to important differences between the present oxides and the previously studied pyrochlores.

Whilst it is likely that the loss of water is correlated with the volume changes, it is interesting that the temperatures of the two processes are not identical. This is illustrated in Fig. 7, and the discrepancy between the two is most apparent in the derivate curves. It appears that the volume contraction commences prior to the loss of the water implying other forces are at play. We return to this point below.

Close examination of the thermal contraction curves, recorded during re-cooling of the sample, illustrated in Fig. 6 shows the presence of a small anomaly near 200 °C for the Ca-containing oxide. Since the sample was maintained under a dynamic vacuum during these measurements, this feature is not associated with the movement of water into the cell. Further studies are required to understand this feature of the thermal expansion of $Sr_2CaSbO_{5.5}$, but we tentatively postulate that it is associated with the distribution of the anion vacancies.

Reheating a sample of $Sr_3SbO_{5.5}$ immediately after cooling to room temperature resulted in linear thermal expansion to 500 °C, there being a dramatic reduction in the anomalous thermal expansion near 250 °C. These results are summarised in Fig. 8. Upon standing for several weeks in the laboratory the sample apparently re-adsorbed water and, once again the anomaly in the thermal expansion was observed. Evidently the sample can re-absorb water upon standing.

There are at least three feasible explanations for this unexpected observation. Firstly the TGA studies demonstrate the presence of at least two types of water molecules, namely those chemisorbed on the surface and those incorporated in the bulk. It is possible that initial anomalous expansion of the lattice near 250 °C is a result of the surface water being incorporated into the lattice. As the temperature is further increased this water is then lost. Colomban et al. [28] have observed, using a combination of vibrational spectroscopy and TGA methods, such a phenomenon in the related oxides $Sr_3TaO_{5.5}$ and $Ba_2CaNbO_{5.5}$. To test this hypothesis a sample of $Sr_3SbO_{5.5}nH_2O$ was mounted in the XRK chamber and a vacuum of $\sim10^{-3}$ Torr established. The sample was next heated from 30 to 110 °C, collecting data at 10° temperature intervals after which time the sample was annealed at 110 °C for 16 h. The TGA studies indicate that such conditions

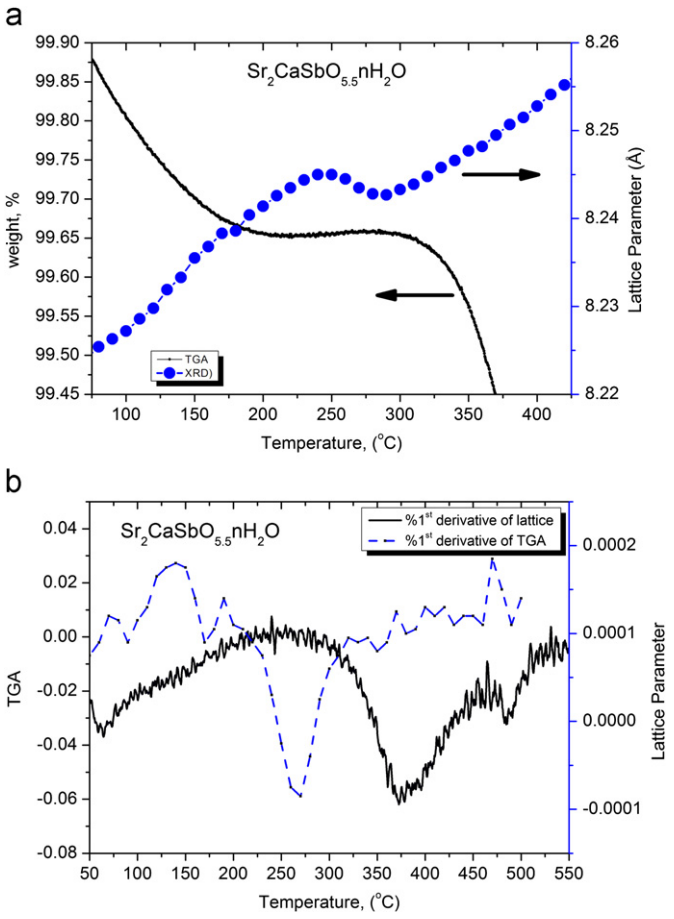

Fig. 7. (a) Temperature dependence of the lattice parameters (XRD measurements recorded with increasing temperature) and weight loss (TGA measurements) for $Sr_2CaSbO_{5.5}nH_2O$. (b) First derivatives of the thermal expansion of the unit cell parameters and weight loss for $Sr_2CaSbO_{5.5}nH_2O$, demonstrating the change in cell volume precedes the loss of water.

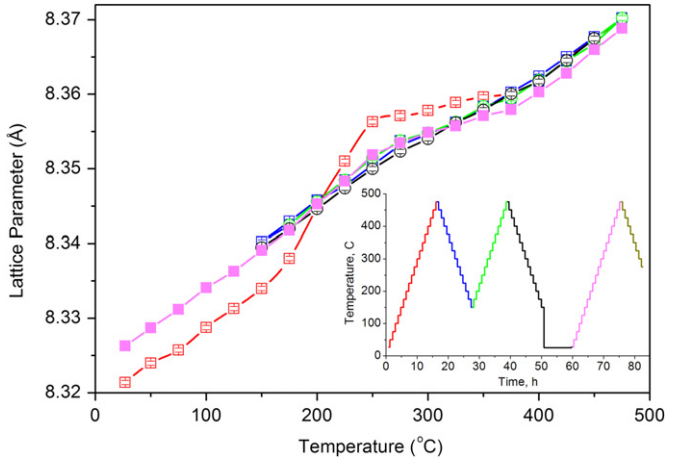

Fig. 8. Influence of thermal cycling on the lattice parameters of $Sr_3SbO_{5.5}nH_2O$. The inset illustrates the thermal profile used. Note the persistence in the anomalous expansion of the cell parameters after re-cooling the sample.

would be sufficient to remove any water present on the surface of the particles, but would not remove any incorporated water. Diffraction patterns were recorded every 30 min during the annealing process and it was observed that the lattice parameter remained essentially constant during this period. The sample was then heated to 500 °C collecting data in 10° temperature steps as before. Again an increase in the rate of thermal expansion was observed near 250 °C. This was followed by a small plateau, before the approximately liner thermal expansion resumed as the sample was heated above 350 °C. The plateau presumably arises since the rate of thermal expansion coincidently corresponds to the contraction resulting from the loss of water. Evidently the altered rate of thermal expansion near 250 °C is not due to the insertion of chemisorbed water into the sample. Once the water is lost the samples exhibit typical thermal expansion and there is no hysteresis in the lattice parameters until the temperature reaches the point where the water loss occurred. Since the sample is under vacuum it cannot re-absorb water but nevertheless there is a small deviation in the rate of contraction of the cell parameter near this point.

A second possible explanation is that the presence of a small amount of water in the lattice somehow induces a contraction of the lattice and that upon loss of the water the lattice actually returns to the "expected" larger value. The data results illustrated in Fig. 6 suggest that may be feasible for the Sr compound but it does not account for the anomaly in the Ba and Ca containing oxides.

The final explanation we considered is that the anomaly in the thermal expansion is not simply a result of the loss of water, but rather it is also influenced by the disorder of the oxygen vacancies. To test the feasibility of this hypothesis a sample of $Sr_3SbO_{5.5}$ was annealed at 800 °C and then slowly cooled under a dry atmosphere to room temperature and promptly mounted in the vacuum of the XRK chamber. In this way it was hoped to avoid the absorption of water from the environment. The diffraction data again showed an anomaly near 250 °C upon heating, confirming that this is not a consequence of the loss of water, and as noted above the neutron profiles demonstrate that the disorder of the anions persists in the absence of the water. The importance of the anion vacancies is clearly demonstrated in the thermal expansion of $Sr_2CaSbO_{5.5}$ where a clear anomaly is observed upon cooling the sample from 500 °C (see Fig. 6). We believe that the combination of anion disorder and the mobility of water in the structure is responsible for the observed thermal expansion behaviour. Irvine and co-workers have observed anomalous variations in the unit cell parameters of some doped cerium based perovskites $ACeO_{3-\delta}$ [29,30]. Focusing on the extent of hydration, they concluded that hydration was reduced as a consequence of defect association and reasoned that site disordering or defect association is likely to introduce strains to the lattice, similar to those introduced by cooperative tilting of the octahedra. Such strains can have a significant effect on the cell volume [31] in addition to the structure of the material [32]. It appears likely that the shape and volume of the water clusters encapsulated within the structure will be dependent on a combination of factors including the distribution of defect clusters, water–water and water–host hydrogen bonds, such that the volume expansion is not simply dependent on the quantity of water incorporated into the structure [33].

As noted above the initial anomaly in the thermal expansion precedes the loss of water. We postulate that this corresponds to a relaxation of the structure including the anion disorder and water clusters and that the water is then lost from this relaxed structure. The synergy between anion disorder and the mobility of water in the structure is probably not unanticipated since the H-atoms from the water molecule will most probably be involved in H-bonding with the oxygen atoms in the perovskite framework. Unfortunately the strongly structured background has prevented us from locating the H-atoms. Complex conductivity behaviour has been observed in related oxides such as $Sr_3TaO_{5.5}$ [15] and $Ba_2CaNbO_{5.5}$ [16] apparently as a consequence of order–disorder transitions involving the *B*-site cations, oxide-ion vacancies and protons. It is likely that the

observed structural behaviour is correlated with a similar phenomenon. There is now evidence that vacancies tend to order in doped zirconias with fluorite-type structures and that vacancy–vacancy interactions can distort the structure [34]. This may also occur in anion deficient perovskites. Irrespective of the precise mechanism it appears that the water reduces cation–cation repulsions leading to a small decrease in the lattice parameters.

4. Conclusions

The average structures of the three oxides $Sr_2BSbO_{5.5}$ have been established from a combination of neutron and synchrotron X-ray diffraction measurements. Synchrotron X-ray diffraction measurements have confirmed the presence of rock-salt like ordering of Sr and Sb in the oxygen deficient perovskite $Sr_3SbO_{5.5}$. In the double perovskite structure it is anticipated that the two smallest cations will order in the octahedral sites, this ordering being a consequence of the differences in the size and/or charge between the two cations. The largest cation will then occupy the 12-coordinate (cuboctahedral) site. For $Sr_2CaSbO_{5.5}$ the Ca^{2+} and Sb^{5+} cations will occupy the 6-coordinate sites and the Sr^{2+} the 12 coordinate sites. In $Sr_2BaSbO_{5.5}$ the Sb^{5+} and one Sr^{2+} occupy the 6-coordinate sites and the cuboctahedral sites are occupied by a mixture of Sr^{2+} and Ba^{2+}. The presence of displacive disorder of the A-site cations and some of the anions reduces the sever underbonding of these cations that would otherwise occur. It is postulated that a combination of defect clusters, water–water and water–host hydrogen bonds, will play a role in defining the shape and volume of the encapsulated water clusters and that the loss of water molecules upon heating results in anomalous thermal expansion and contraction behaviour.

Acknowledgments

BJK acknowledges the support of the Australian Research Council for this work. The work performed at the Australian National Beamline Facility was supported by the Australian Synchrotron Research Program, which is funded by the Commonwealth of Australia under the Major National Research Facilities program. The assistance of Dr. James Hester at the ANBF is gratefully acknowledged. We thank the editor for insightful comments on this manuscript.

References

[1] R. Glockner, M.S. Islam, T. Norby, Solid State Ion. 122 (1999) 145–156.
[2] T. Norby, J. Mater. Chem. 11 (2001) 11–18.
[3] Y.H. Huang, R.I. Dass, Z.L. Xing, J.B. Goodenough, Science 312 (2006) 254–257.
[4] E. Kendrick, K.S. Knight, M.S. Islam, P.R. Slater, Solid State Ion. 178 (2007) 943–949.
[5] T. Nagasaki, T. Ito, M. Yoshino, K. Iwasaki, S. Shiotani, H. Fukazawa, N. Igawa, Y. Ishii, J. Nucl. Sci. Technol. (2008) 122–127.
[6] R. Glockner, A. Neiman, Y. Larring, T. Norby, Solid State Ion. 125 (1999) 369–376.
[7] K. Yoshioka, V. Petrykin, M. Kakihana, H. Kato, A. Kudo, J. Catal. 232 (2005) 102–107.
[8] Q.D. Zhou, B.J. Kennedy, J. Solid State Chem. 177 (2004) 654–659.
[9] G. King, A.M. Abakumov, J. Hadermann, A.M. Alekseeva, M.G. Rozova, T. Perkisas, P.M. Woodward, G. Van Tendeloo, E.V. Antipov, Inorg. Chem. 49 (2010) 6058–6065.
[10] E.G. Steward, H.P. Rooksby, Acta Crystallogr. 4 (1951) 503.
[11] I. Levin, J.Y. Chan, J.H. Scott, L. Farber, T.A. Vanderah, J.E. Maslar, J. Solid State Chem. 166 (2002) 24–41.
[12] M.R. Li, S.T. Hong, Chem. Mater. 20 (2008) 2736–2741.
[13] A. Ashok, N. Kochetova, T. Norby, A. Olsen, Solid State Ion. 179 (2008) 1858–1866.
[14] N. Jalarvo, C. Haavik, C. Kongshaug, P. Norby, T. Norby, Solid State Ion. 180 (2009) 1151–1156.
[15] I. Animitsa, A. Neiman, N. Kochetova, B. Melekh, A. Sharafutdinov, Solid State Ion. 162 (2003) 63–71.
[16] I. Animitsa, A. Neiman, A. Sharafutdinov, S. Nochrin, Solid State Ion. 136 (2000) 265–271.
[17] M. Saidi, E. Moran, U. Amador, M. Abboudi, A. Asskali, Mater. Res. Bull. 35 (2000) 1269–1275.
[18] E. Chinarro, G.C. Mather, A. Caballero, M. Saidi, E. Moran, Solid State Sci. 10 (2008) 645–650.
[19] B.A. Hunter, C.J. Howard, RIETICA. A Computer Program for Rietveld Analysis of X-Ray and Neutron Powder Diffraction Patterns, 1998.
[20] T.M. Sabine, B.J. Kennedy, R.F. Garrett, G.J. Foran, D.J. Cookson, J. Appl. Crystallogr. 28 (1995) 513–517.
[21] K.D. Liss, B. Hunter, M. Hagen, T. Noakes, S. Kennedy, Phys. B-Condens. Matter 385-86 (2006) 1010–1012.
[22] R.D. Shannon, Acta Crystallogr. A 32 (1976) 751–767.
[23] P.J. Saines, B.J. Kennedy, M.M. Elcombe, H.H. Harris, L.Y. Jang, Z.M. Zhang, J. Solid State Chem. 181 (2008) 2941–2952.
[24] Y. Kuroiwa, H. Fujiwara, A. Sawada, S. Aoyagi, E. Nishibori, M. Sakata, M. Takata, H. Kawaji, T. Atake, Jpn. J. Appl. Phys. Part 1—Regul. Pap. Short Notes Rev. Pap. 43 (2004) 6799–6802.
[25] S.T. Hong, J. Solid State Chem. 180 (2007) 3039–3048.
[26] I. Levin, J.C. Woicik, A. Llobet, M.G. Tucker, V. Krayzman, J. Pokorny, I.M. Reaney, Chem. Mater. 22 (2010) 4987–4995.
[27] G.J. Thorogood, B.J. Kennedy, V. Luca, M. Blackford, S.K. van de Geest, K.S. Finnie, J.V. Hanna, K.J. Pike, J. Phys. Chem. Solids 69 (2008) 1632–1640.
[28] P. Colomban, F. Romain, A. Neiman, I. Animitsa, Solid State Ion. 145 (2001) 339–347.
[29] A. Kruth, R.A. Davies, M.S. Islam, J.T.S. Irvine, Chem. Mater. 19 (2007) 1239–1248.
[30] A. Kruth, G.C. Mather, J.R. Jurado, J.T.S. Irvine, Solid State Ion. 176 (2005) 703–712.
[31] M.A. Carpenter, R.E.A. McKnight, C.J. Howard, Q.D. Zhou, B.J. Kennedy, K.S. Knight, Phys. Rev. B 80 (2009) 214101.
[32] Q.D. Zhou, P.J. Saines, N. Sharma, J. Ting, B.J. Kennedy, Z.M. Zhang, R.L. Withers, K.S. Wallwork, Chem. Mater. 20 (2008) 6666–6676.
[33] N. Guillou, F. Millange, R.I. Walton, Chem. Commun. 47 (2011) 713–715.
[34] D. Marrocchelli, P.A. Madden, S.T. Norberg, S. Hull, Chem. Mater. 10.1021/cm102809t (2011).